

Action Potential Clamp and Pharmacology of the Variant 1 Short QT Syndrome T618I hERG K⁺ Channel

Aziza El Harchi¹, Dario Melgari¹, Yi Hong Zhang¹, Henggui Zhang², Jules C. Hancox^{1*}

1 School of Physiology and Pharmacology and Cardiovascular Research Laboratories, University of Bristol, Bristol, United Kingdom, **2** Biological Physics Group, School of Physics and Astronomy, The University of Manchester, Manchester, United Kingdom

Abstract

Background: The familial Short QT Syndrome (SQTS) is associated with an increased risk of cardiac arrhythmia and sudden death. Gain-of-function mutations in the hERG K⁺ channel protein have been linked to variant 1 of the SQTS. A hERG channel pore (T618I) mutation has recently been identified in families with heritable SQTS. This study aimed to determine effects of the T618I-hERG mutation on (i) hERG current (I_{hERG}) elicited by ventricular action potentials; (ii) the sensitivity of I_{hERG} to inhibition by four clinically used antiarrhythmic drugs.

Methods: Electrophysiological recordings of I_{hERG} were made at 37°C from HEK 293 cells expressing wild-type (WT) or T618I hERG. Whole-cell patch clamp recording was performed using both conventional voltage clamp and ventricular action potential (AP) clamp methods.

Results: Under conventional voltage-clamp, WT I_{hERG} peaked at 0–+10 mV, whilst for T618I I_{hERG} maximal current was rightward shifted to ~ +40 mV. Voltage-dependent activation and inactivation of T618I I_{hERG} were positively shifted (respectively by +15 and ~ +25 mV) compared to WT I_{hERG} . The I_{hERG} ‘window’ was increased for T618I compared to WT hERG. Under ventricular AP clamp, maximal repolarising WT I_{hERG} occurred at ~ -30 mV, whilst for T618I hERG peak I_{hERG} occurred earlier during AP repolarisation, at ~ +5 mV. Under conventional voltage clamp, half-maximal inhibitory concentrations (IC_{50}) for inhibition of I_{hERG} tails by quinidine, disopyramide, D-sotalol and flecainide for T618I hERG ranged between 1.4 and 3.2 fold that for WT hERG. Under action potential voltage clamp, T618I IC_{50} s ranged from 1.2 to 2.0 fold the corresponding IC_{50} values for WT hERG.

Conclusions: The T618I mutation produces a more modest effect on repolarising I_{hERG} than reported previously for the N588K-hERG variant 1 SQTS mutation. All drugs studied here appear substantially to retain their ability to inhibit I_{hERG} in the setting of the SQTS-linked T618I mutation.

Citation: El Harchi A, Melgari D, Zhang YH, Zhang H, Hancox JC (2012) Action Potential Clamp and Pharmacology of the Variant 1 Short QT Syndrome T618I hERG K⁺ Channel. PLoS ONE 7(12): e52451. doi:10.1371/journal.pone.0052451

Editor: Bernard Attali, Sackler Medical School, Tel Aviv University, Israel

Received: June 27, 2012; **Accepted:** November 14, 2012; **Published:** December 26, 2012

Copyright: © 2012 El Harchi et al. This is an open-access article distributed under the terms of the Creative Commons Attribution License, which permits unrestricted use, distribution, and reproduction in any medium, provided the original author and source are credited.

Funding: The authors thank the British Heart Foundation for funding (AEH: PG/10/96; DM: FS/11/59; YZ: PG/10/17). The funders had no role in study design, data collection and analysis, decision to publish, or preparation of the manuscript.

Competing Interests: The authors have declared that no competing interests exist.

* E-mail: Jules.hancox@bristol.ac.uk

Introduction

The rapid delayed rectifier K⁺ channel current (I_{Kr}) is an important determinant of ventricular AP repolarisation and, consequently, of the duration of the QT interval on the electrocardiogram [1,2]. Channels mediating I_{Kr} are formed by proteins encoded by *hERG* (*human Ether-à-go-go Related Gene*; alternative nomenclature *KCNH2* [3,4]). Native I_{Kr} and hERG channels exhibit sensitivity to pharmacological blockade by diverse drugs, including both Class Ia and Class III antiarrhythmic agents; excessive pharmacological inhibition of I_{Kr} /hERG leads to acquired long QT syndrome (LQTS [5–8]). Loss-of-function *KCNH2* mutations are responsible for the LQT2 form of heritable long QT syndrome [9,10], whilst gain-of-function mutations are responsible for the SQT1 form of heritable Short QT syndrome (SQTS [11,12]).

The *KCNH2* mutations first identified in SQTS patients led to a common asparagine to lysine (N→K) substitution within the

external S5-Pore linker region of the hERG channel protein [13,14]. hERG current (I_{hERG}) carried by N588K-hERG mutant channels failed to rectify normally, due to a substantial (+60 to +90 mV) rightward shift in voltage-dependent inactivation [13,15,16]. The use *in vitro* of the action potential (AP) voltage clamp technique showed that the impaired inactivation of N588K hERG channels altered significantly the profile of I_{hERG} during the plateau and repolarisation phases of ventricular APs, leading to increased I_{hERG} occurring much earlier during the ventricular AP waveform [13,15,16]. Additionally, SQT1 patients with the N588K mutation were found to be refractory to treatment with Class III antiarrhythmic drugs (sotalol, ibutilide), but did respond to the Class Ia agents quinidine and disopyramide [13,17–19]. This differential influence of the N588K mutation on clinical effectiveness of Class Ia and III drugs correlates with changes in I_{hERG} blocking potency seen *in vitro* [13,18,20] and is explicable on the basis of the comparatively greater dependence of Class III than Class Ia drugs on I_{hERG} inactivation in order to bind to the

channel [21]. A second gain-of-function hERG mutation, identified in the S5 domain of zebrafish ERG (zERG; L499P; hERG homologue L532P) in *reggae* mutant zebrafish with accelerated cardiac repolarisation [22], has been found to produce marked kinetic alterations including to voltage and time-dependent inactivation [22,23]. The L532P hERG homologue also exhibits altered sensitivity to Class III drug block [23].

Recently, a novel SQT1 mutant has been identified in a Chinese family with a history of nocturnal sudden death [24]. Four of eleven family members evaluated exhibited shortened rate-corrected QT intervals (with a mean QT_c interval of 316 ms) [24]. Genotyping of the proband identified a base transition (C1853T) that led to a threonine to isoleucine substitution at position 618 (located in the hERG channel pore helix) of hERG; this was absent in 200 ethnically matched controls [24]. *In vitro* biophysical analysis identified significant alterations to I_{hERG} kinetics, including a ~+50 mV shift in voltage dependent inactivation [24]. Pharmacological experiments with single high concentrations of quinidine or sotalol (producing 70% or greater inhibition of wild-type (WT) I_{hERG}) were suggestive of retained I_{hERG} block of T618I hERG during applied voltage commands [24]. At present, however, concentration-response data for pharmacological inhibition of T618I hERG appear to be lacking for any drug. Moreover, the effect of the T618I mutation on the profile of I_{hERG} during dynamic physiological waveforms (ventricular APs) has not yet been reported. The present study was conducted to address both of these issues, through experiments on recombinant WT and T618I channel I_{hERG} conducted at human physiological temperature.

Materials and Methods

Wild-type and T618I hERG

Human Embryonic Kidney (HEK-293) cells stably expressing WT hERG were donated by Prof Craig January [25]. HEK 293 cells used for transient transfection were obtained from ECCAC (catalog number 85120602). The T618I mutant was constructed using QuikChange® (Stratagene) mutagenesis. The following forward primer sequence was used: 5'CGG CGC TCT ACT TCA TCT TCA GCA GCC TCAC3'. DNA was sequenced for the full length of the hERG insert to ensure that only the correct mutation had been made (Eurofins MWG Operon).

Maintenance of Cells and Cell Transfection

Experiments employed HEK-293 cells stably or transiently expressing WT or T618I hERG constructs. Cells were passaged and maintained as described previously [23,26]. For transient transfection experiments, 24 hours after plating cells out they were transiently transfected with 0.3 µg of T618I hERG construct using Lipofectamine™ LTX (Invitrogen) according to the manufacturer's instructions. Expression plasmid encoding CD8 was also added as a transfection marker [26]. Cells were plated onto small sterilised collagen-coated glass coverslips 6 hours after transfection and recordings were made after at least 24 hours incubation at 37°C. Successfully transfected cells were identified using Dynabeads® (Invitrogen).

Electrophysiology

Once in the recording chamber, cells were superfused at 37°C with an external solution containing (in mM): 140 NaCl, 4 KCl, 2.5 CaCl₂, 1 MgCl₂, 10 Glucose and 5 HEPES (titrated to pH 7.45 with NaOH). Patch-pipettes (Corning 7052 glass, AM Systems) were pulled and heat-polished (Narishige MF83) to 2.5–4 MΩ; pipette dialysate contained (in mM): 130 KCl, 1 MgCl₂, 5

EGTA, 5 MgATP, 10 HEPES (titrated to pH 7.2 using KOH) [26;27]. hERG current (I_{hERG}) recordings were made using an Axopatch 200, 200A or 200B amplifier (Axon Instruments, now Molecular Devices) and a CV201, CV202A or CV203BU headstage. Between 70–80% of pipette series resistance was compensated. Voltage-clamp commands were generated and data recorded using 'WinWCP' (John Dempster, Strathclyde University) or pClamp 9.0 and 10.0 (Molecular Devices). The ventricular action potential (AP) command used for AP clamp experiments was identical to that used in other recent studies from our laboratory [23,27].

Drugs

Disopyramide-phosphate powder (Sigma-Aldrich) was dissolved in Milli-Q water to produce an initial stock solution of 400 mM which was diluted further to produce stock solutions ranging down to 1 mM. Quinidine gluconate salt (Sigma-Aldrich) was dissolved in MilliQ water to produce an initial stock solution of 100 mM, which was diluted further to produce stock solutions ranging down to 30 µM. Flecainide acetate salt (Sigma-Aldrich) was dissolved in MilliQ water to produce an initial stock solution of 10 mM, which was diluted further to produce stock solutions ranging down to 1 mM. D-sotalol (Sequoia) was dissolved in DMSO to produce an initial stock solution of 100 mM, with further dilution of stocks to solutions ranging down to 10 µM. Disopyramide and quinidine containing stock solutions were diluted at least 1:1000-fold with Tyrode's solution to achieve the final concentrations stated in the Results text. For D-sotalol, dilutions of 1:1000 fold were achievable for all final concentrations except 500 µM, for which a dilution of only 5:1000 fold was possible. During recordings all external solutions were applied using a home-built, warmed and rapid solution exchange device [28].

Data Analysis

Concentration-response data were fitted by a standard Hill equation in order to obtain half-maximal inhibitory concentration (IC₅₀) and Hill-coefficient (n_H) values (±95% confidence intervals (C.I.)). Mean data are otherwise presented as mean ± SEM. The voltage dependence of I_{hERG} activation was determined by fitting the values of I_{hERG} tail currents (normalised to peak I_{hERG} tail value and plotted against voltage) with a Boltzmann equation of the form:

$$I = I_{Max} / (1 + \exp[(V_{0.5} - V_m) / k]) \quad (1)$$

where I is the I_{hERG} tail amplitude following test potential V_m, I_{Max} is the maximal I_{hERG} tail observed during the protocol, V_{0.5} is the potential at which I_{hERG} was half-maximally activated, and k is the slope factor for the relationship.

The voltage dependence of I_{hERG} inactivation (assessed by studying availability) was determined by fitting normalised peak I_{hERG} currents elicited by the third step of a three-step protocol (Figure 3A) by the equation:

$$I / I_{Max} = 1 - (1 + \exp[(V_{0.5} - V_m) / k]) \quad (2)$$

where I = transient current elicited by the third step of the protocol, following a brief (2 ms) conditioning step (V_m) to relieve inactivation induced by the first step; I_{Max} is the maximal transient current observed during the protocol and V_{0.5} and k denote, respectively, half-maximal inactivation voltage and slope factor for the fit to the plotted relation.

Statistical analysis (SigmaPlot 12) utilised, as appropriate, an unpaired t-test, a Welch's t-test not assuming equal variances, or a two way repeated measures ANOVA test. *P* values of less than 0.05 were taken as statistically significant.

Results

Effects of the T618I hERG Mutation on the Voltage-dependence of I_{hERG} and its Activation

Figures 1Ai and Aii show representative current traces for WT and T618I I_{hERG} elicited by the voltage protocol shown in the lower panels (Figures 1Bi and Bii). WT I_{hERG} increased progressively with the magnitude of the applied voltage commands up to $\sim 0/+10$ mV, positive to which the current during the applied command declined in amplitude. Prominent I_{hERG} tails were observed on repolarisation to -40 mV after each voltage command, with tail current amplitude exceeding that of the preceding current during the depolarising step, particularly for positive command voltages. These features are typical of WT I_{hERG} [3,4,25,29]. The traces shown in Figure 1Aii indicate that at potentials negative to 0 mV, T618I I_{hERG} resembled WT I_{hERG} . However, at test potentials between ~ 0 and $+40$ mV (over which WT I_{hERG} elicited by depolarising commands became reduced in amplitude), T618I I_{hERG} continued to increase in magnitude. T618I I_{hERG} began to decline in amplitude at test potentials positive to $+40$ mV. Notably, with positive test commands, T618I I_{hERG} did not exhibit tail currents (I_{tails}) that exceeded pulse current in amplitude (*cf* [24]). Figure 1C shows mean end-pulse current voltage (*I-V*) relations for WT and T618I I_{hERG} , demonstrating maximal current for WT I_{hERG} at $\sim +10$ mV and an area of negative slope in the *I-V* relation at more positive potentials. For T618I hERG, rectification of the *I-V* relation was positively voltage-shifted, with the area of negative slope in the *I-V* relation occurring positive to $+40$ mV. Figure 1D shows mean normalised *I-V* relations for WT and T618I hERG I_{tails} , fitted with equation 1 (Methods). For WT I_{hERG} the mean activation $V_{0.5}$ was -23.1 ± 1.5 mV ($n=6$), whilst for T618I I_{hERG} this was -8.0 ± 3.4 mV ($n=7$; $p<0.01$ versus WT). The corresponding *k* values were 7.8 ± 1.5 and 8.5 ± 0.9 mV respectively ($p>0.05$).

Effects of the T618I Mutation on I_{hERG} Activation and Deactivation Time-course

In order to investigate effects of the T618I mutation on the time-course of I_{hERG} activation, we used an "envelope of tails protocol" in which I_{tails} were measured at -40 mV following activating commands of different durations from -80 to 0 mV (see inset to Fig. 2A). I_{tails} elicited by commands of different duration were normalised to the maximum current during the protocol and plotted as a function of command pulse duration, as shown in Figure 2A (*cf* [23,30]). Mono-exponential fits to the data yielded a $\tau_{activation}$ of 104.1 ± 8.3 ms for WT I_{hERG} and of 112.0 ± 13.0 ms for T618I I_{hERG} ($n=5$ and 6 cells respectively; $p>0.5$), indicating that activation time-course was similar for WT and T618I I_{hERG} during this protocol. In order to compare I_{hERG} deactivation time-course between WT and T618I hERG, I_{tails} elicited at -40 mV following voltage commands to $+20$ mV were fitted with a standard bi-exponential function. Figures 2Bi and Bii show respectively the mean fast and slow time-constants of deactivation (τ_f 'fast tau' and τ_s 'slow tau', respectively) for WT and T618I I_{hERG} . Both fast and slow phases of deactivation were faster for T618I than WT I_{hERG} (evidenced by smaller tau values plotted in Figure 2B; $p<0.05$ and $p<0.01$ respectively for τ_f and τ_s versus WT). However, the relative proportion of fast and slow deactivation did not differ between WT and T618I I_{hERG}

(quantified in Figure 2C as proportion of total deactivating current described by τ_f).

Effects of the T618I hERG Mutation on I_{hERG} Inactivation

In order to characterize the effect of the T618I mutation on the voltage-dependence of I_{hERG} inactivation, voltage dependent availability of I_{hERG} was determined for WT- and T618I-hERG by applying voltage protocols used in prior investigations from our laboratory to study effects on inactivation of gain-of-function hERG mutations [16,23]. These were comprised of an initial (500 ms) depolarizing step to activate and then fully inactivate I_{hERG} , followed by brief (2 ms) repolarizing steps to a range of potentials to relieve inactivation to varying extents, followed by a third depolarization step that elicited a rapidly inactivating I_{hERG} . The magnitude of peak current elicited by the third step reflected the extent of availability induced by the (second) repolarizing step. Similar to prior studies of gain-of-function hERG mutations performed in our laboratory [16,23], in order to ensure complete inactivation of I_{hERG} during the initial step of the voltage protocol, for T618I I_{hERG} a depolarizing step to $+80$ mV was used, compared to $+40$ mV for WT I_{hERG} . The lower panels of Figures 3Ai and Aii show the portion of the protocol that incorporated the repolarizing step and subsequent depolarization phases, with the upper panels showing corresponding I_{hERG} records. Peak current amplitudes were obtained by fitting the declining phase of the transient I_{hERG} records with a mono-exponential function and extrapolation to the beginning of the third pulse [16,23]. The resulting values were normalized to the maximal current seen during the protocol and were plotted against repolarization step voltage. The availability/inactivation $V_{0.5}$ value for WT I_{hERG} derived from a fit to the data with equation 2 was -65.5 ± 2.2 mV with a *k* value of 19.8 ± 0.6 ($n=11$ cells). For T618I I_{hERG} , the corresponding values were: $V_{0.5}$ of -40.7 ± 5.1 mV and *k* of 26.9 ± 1.9 mV ($n=6$ cells; and, respectively, $p<0.01$ and 0.001 versus control). For the sake of completeness, the data were further analysed by correction for deactivation using the method of Smith et al. [31] then plotted against voltage and fitted with equation 2 (Figure 3B), which gave $V_{0.5}$ values of -67.2 ± 2.0 and -44.3 ± 5.1 mV respectively for WT and T618I I_{hERG} ($p<0.01$) and respective *k* values of 21.0 ± 0.6 and 29.8 ± 1.7 mV ($P<0.001$). Thus, I_{hERG} inactivation $V_{0.5}$ was positively shifted by $\sim +23$ to $+25$ mV for T618I I_{hERG} compared to WT I_{hERG} , with an accompanying 7 to 9 mV increase in *k* value. In order to establish the overall effects of altered steady-state voltage-dependent kinetics of the T618I mutation, we calculated 'window current' for WT and T618I hERG, as the activation-inactivation variable product across a range of voltages between -80 and $+60$ mV. Figure 3C shows that the I_{hERG} window was both positively shifted and significantly larger for T618I than WT I_{hERG} .

The time-course of development of inactivation for WT and T618I I_{hERG} was compared by mono-exponential fitting of the decline of transient currents elicited following the repolarizing step to -140 mV. This yielded τ -values for WT and T618I I_{hERG} inactivation of 1.86 ± 0.17 ms and 3.32 ± 0.28 ms respectively (Figure 3D; $n=11$ and 6 respectively; $p<0.01$). To compare the rate of recovery from inactivation between the two channels, we used a protocol used in prior I_{hERG} studies ([23,30] see also inset of Figure 3E): a 500-ms depolarisation to $+40$ mV was applied from a holding potential of -80 mV to activate and inactivate I_{hERG} . Membrane potential was then repolarised to -40 mV for an increasing periods of time (between 2 and 20 ms) to induce recovery from inactivation. Transient currents were then subsequently elicited by a 100-ms depolarisation to $+40$ mV.

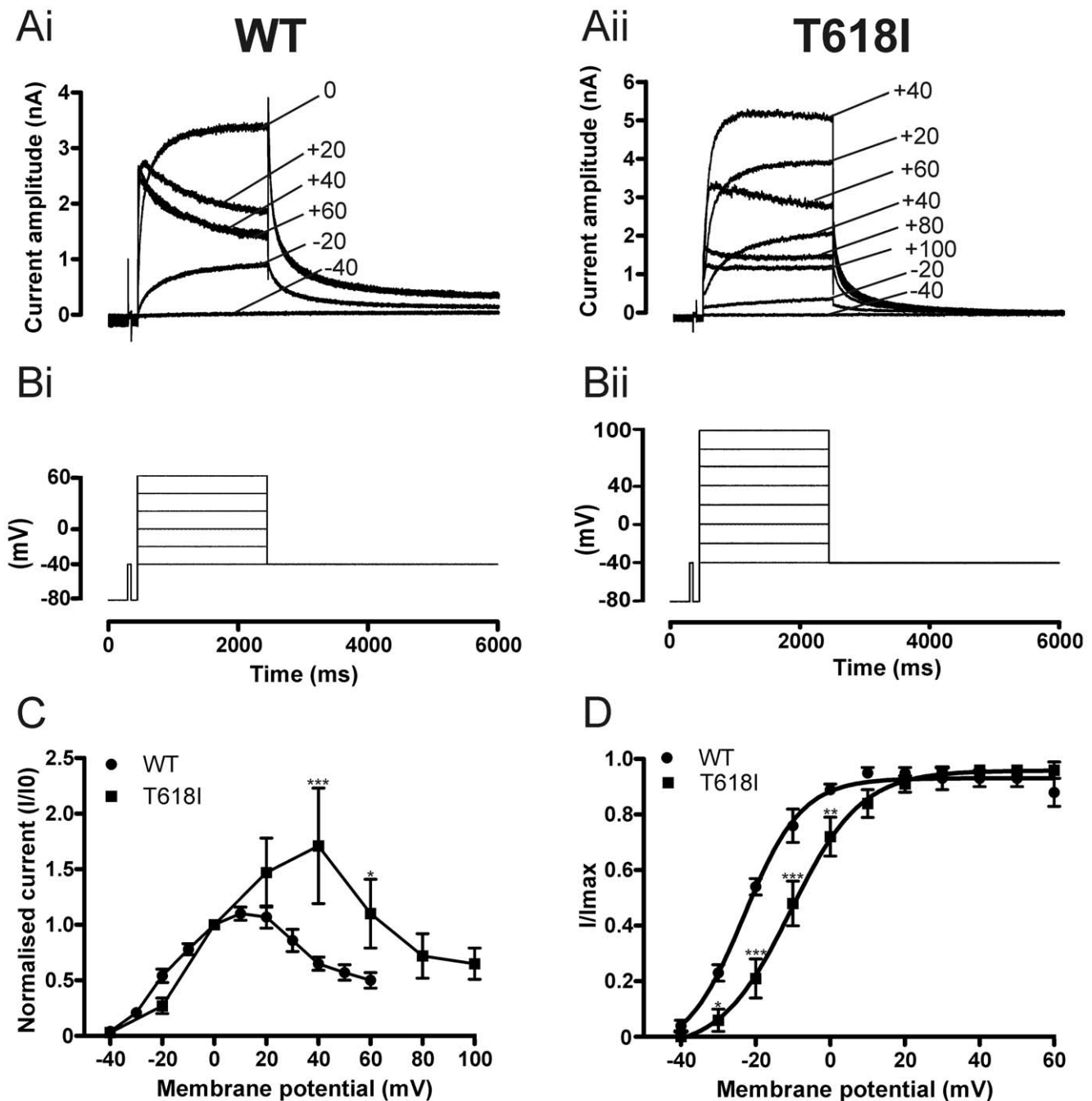


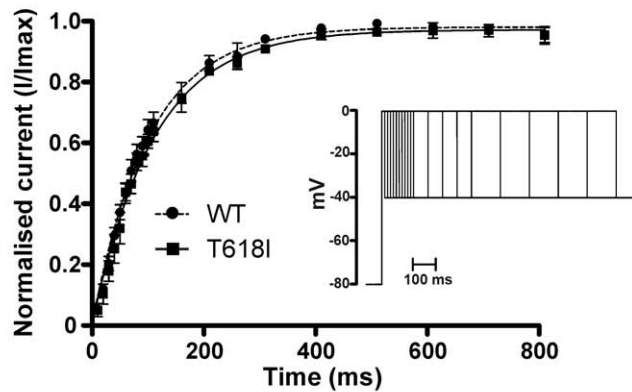
Figure 1. Basic characteristics of T618I I_{hERG} . (A,B) Upper traces (A) show representative current records for WT I_{hERG} (Ai) and T618I I_{hERG} (Aii) elicited by voltage protocols shown in B (Bi - WT and Bii - T618I); note that for WT I_{hERG} measurements, successive voltage steps increased by 10 mV increments up to +60 mV, whilst for T618I I_{hERG} successive steps increased by 20 mV up to +100 mV. Note that for clarity of display only selected traces elicited by the protocol are shown. Numbers in Ai and Aii indicate command voltage at which currents recorded. Note different current scales in Ai and Aii. (C) Current voltage (I-V) relations for WT (n=6) and T618I (n=5) I_{hERG} elicited by the voltage protocol shown in panel B. Data are shown for end pulse I-V relations, in which currents for each cell studied were normalized to the current value at 0 mV. (D) I-V relations for WT (n=6) and T618I (n=7) tail current recorded at -40 mV following repolarisation from the test potentials plotted on the membrane potential axis (for these measurements I_{hERG} tails were measured following depolarising steps to potentials between -40 and +60 mV (in 10 mV increments)). Tail currents were measured relative to the instantaneous current elicited by the brief (50 ms) step from -80 to -40 mV prior to the applied voltage commands. Data were fitted by equation 1, to give the $V_{0.5}$ and k values in the Results text. Asterisks in C and D denote statistical significance: * $p < 0.05$; ** $p < 0.01$; *** $p < 0.001$.

doi:10.1371/journal.pone.0052451.g001

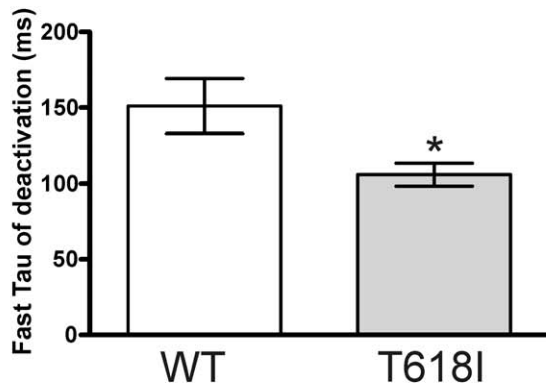
Figure 3E shows plots of WT and T618I peak outward transient current magnitude against the duration of the repolarization step (with currents normalized to maximal current seen during the

protocol). Fits to the data with a mono-exponential function gave τ values of 1.99 ± 0.12 ms for WT (n=7) and of 1.93 ± 0.30 ms for T618I (n=9) ($p > 0.05$).

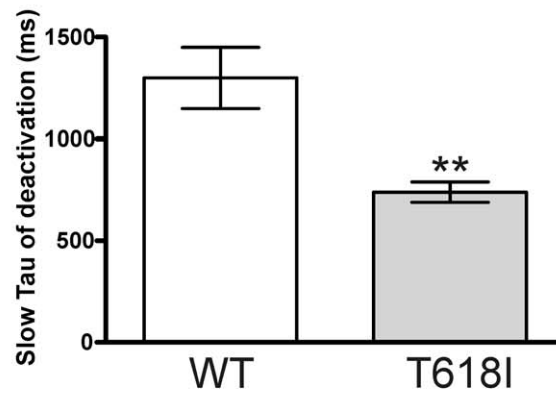
A



Bi



Bii



C

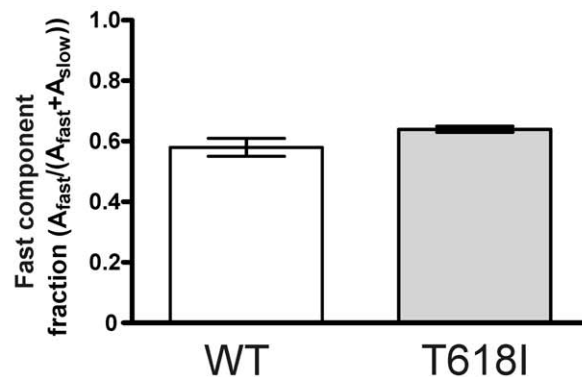


Figure 2. WT and T618I I_{hERG} time-course of activation and deactivation. (A) Plots of time-course of I_{hERG} activation obtained using an “envelope-of-tails” protocol— see inset and ‘Results’ text. For each cell, the peak current amplitudes at each time-point were normalized to the maximal current observed during the protocol. (Bi, Bii) Bar charts comparing τ_f (Bi) and τ_s (Bii) values for deactivation of WT ($n=11$) and T618I ($n=11$) hERG tail currents on repolarisation to -40 mV following a 2 s depolarisation from -80 mV to $+20$ mV. Currents were fitted with a standard bi-exponential equation (C) Bar-chart showing the proportion of fast deactivation on repolarisation to -40 mV for WT and T618I I_{hERG} ($n=11$ cells for each condition). Asterisks in Bi and Bii denote statistical significance: * $p<0.05$; ** $p<0.01$. doi:10.1371/journal.pone.0052451.g002

Collectively, the results from these experiments indicate that the T618I mutation induced a positive shift in the voltage-dependence of I_{hERG} inactivation, augmented the I_{hERG} ‘window’, slowed the

time-course of development of I_{hERG} inactivation, but did not alter significantly the rate of recovery of I_{hERG} from inactivation.

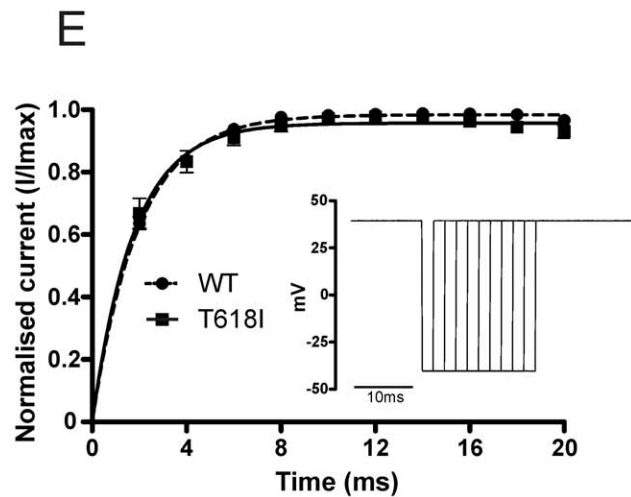
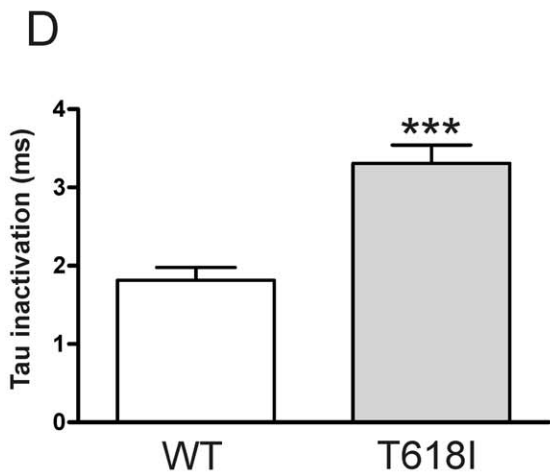
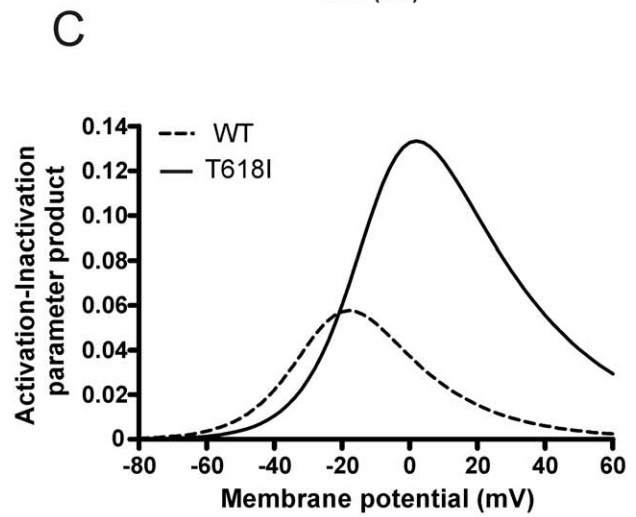
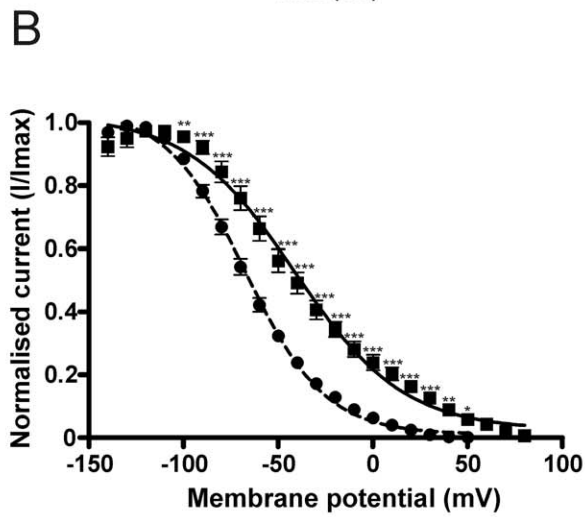
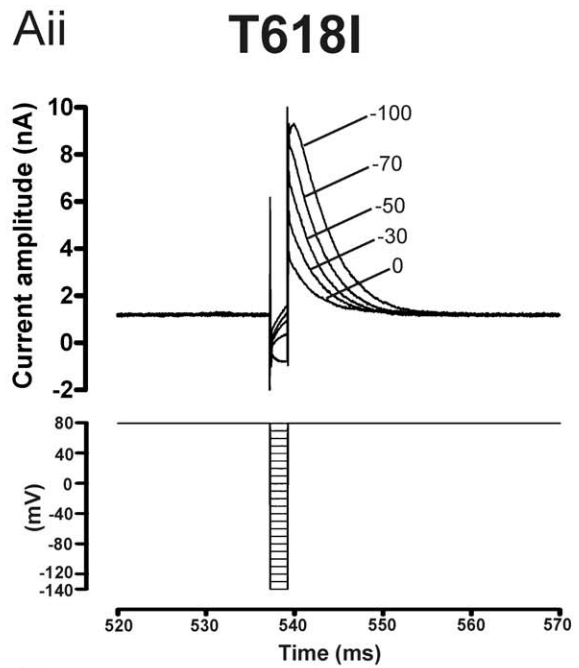
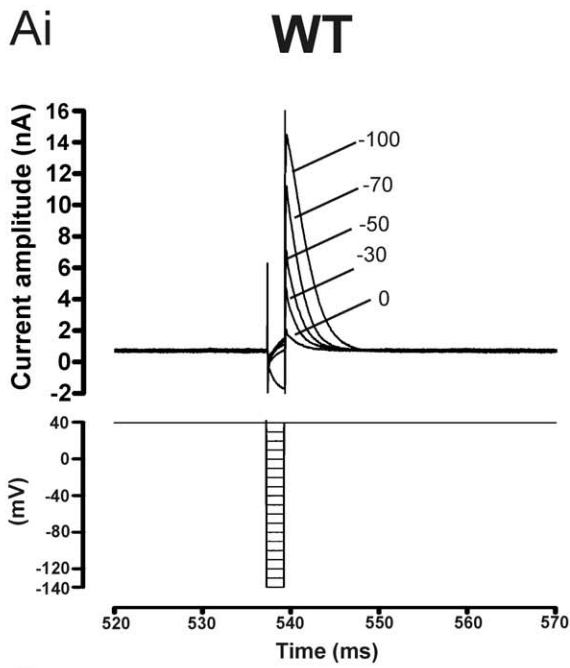


Figure 3. Voltage dependence of WT and T618I I_{hERG} inactivation. (Ai, Aii) Upper traces show representative current records for WT I_{hERG} (Ai) and T618I I_{hERG} (Aii) elicited by voltage protocols shown in lower panels (see also 'Results' text). A more positive voltage (+80 mV) was used for the first and third steps for T618I hERG than for WT hERG (+40 mV) to ensure that complete inactivation occurred on membrane potential depolarisation. Note that for clarity of display only selected traces elicited by the protocol are shown. Numbers in Ai and Aii indicate command voltage at which currents recorded. (B) Plots against voltage (during the second step of the protocol) of I_{hERG} availability. Peak current values and availability plots were constructed as described previously [16], employing deactivation correction as per [31]. A Boltzmann equation fit to the data gave a $V_{0.5}$ for inactivation of -67.2 mV ($k=21.0$ mV) for WT and a $V_{0.5}$ of -44.3 mV ($k=29.8$) for T618I ($n=11$ and 6 cells respectively). (C) 'Window current' for WT and T618I hERG. Derived activation and inactivation $V_{0.5}$ and k values from Figures 1D and 3B were used with equations 1 and 2 to calculate activation and inactivation variables at 2 mV intervals between -80 and $+60$ mV. Window I_{hERG} was calculated as the activation-inactivation variable product at each voltage. (D) Bar charts comparing time constant of WT ($n=11$) and T618I ($n=6$) I_{hERG} inactivation, following brief hyperpolarisation to -140 mV. Inactivating currents were fitted with a standard mono-exponential function (E) Recovery from inactivation time-course for WT and T618I hERG (protocol shown as inset). The dashed gray line denotes mono-exponential fit to WT data ($n=7$). The solid line denotes mono-exponential fit to T618I data, with the dotted line connecting these data at successive time points ($n=9$). Asterisks in B and C denote statistical significance: * $p<0.05$; ** $p<0.01$; *** $p<0.001$. doi:10.1371/journal.pone.0052451.g003

Effects of the T618I Mutation on I_{hERG} under Action Potential Voltage Clamp

Figure 4Ai shows a representative record of WT I_{hERG} elicited by a ventricular AP command (superimposed on the current trace in Figure 4Ai). As reported previously (e.g. [25,30,32]), the elicited current was comparatively small immediately on AP depolarisation, then increased progressively during the plateau phase of the AP, before declining during terminal repolarisation. Figure 4Aii shows similar recordings for T618I I_{hERG} . The profile of current during the AP command differed from that for WT I_{hERG} : current increased earlier during the AP command, peaking earlier during the AP plateau and then it declined during the latter part of the plateau phase. Figures 4Bi and Bii show representative normalized instantaneous current-voltage (I - V) relations for I_{hERG} during the repolarising phase of the AP command. Peak outward current was positively shifted by $\sim +35$ mV for T618I I_{hERG} (from -30.7 ± 1.2 mV for WT, to $+5.1\pm 2.1$ mV for T618I hERG; $P<0.001$ versus WT). Example instantaneous conductance-voltage (G - V) relations (cf [16,32,33]) for WT- and T618I-hERG are shown in Figures 4Ci and Cii, respectively. As described previously [16,32,33], the macroscopic conductance of WT-hERG increased throughout the AP repolarisation phase, being maximal late in repolarisation (Figure 4Ci). In contrast, for T618I I_{hERG} conductance increased steeply early in repolarisation (between $\sim +20$ and -20 mV) and then progressively declined as the membrane potential followed the direction of membrane repolarisation. Figure 4D shows mean data for the maximal amplitudes of WT and T618I I_{hERG} during the applied ventricular AP command waveform, demonstrating a significantly greater (~ 2 -fold) maximal repolarising current when hERG channels incorporated the T618I hERG mutation. Considered collectively, the findings from our AP clamp experiments indicate that greater repolarising I_{hERG}/I_{Kr} would be expected to occur earlier during ventricular APs in the setting of T618I-linked SQT1.

Pharmacology of the T618I hERG Mutation

Figure 5A compares the response of WT and T618I I_{hERG} to $1 \mu\text{M}$ of the Class Ia antiarrhythmic drug quinidine, using conventional voltage-clamp. Figures 5Ai and Aii show representative I_{hERG} traces elicited by the voltage protocol shown in the lower panels (a standard depolarising step protocol used in previous studies of I_{hERG} pharmacology from our laboratory (e.g. [23,26,34])). Tail current magnitude was measured relative to instantaneous current at -40 mV elicited by the brief (50 ms) depolarising step that preceded the voltage command to $+20$ mV in the absence and presence of the drug. $1 \mu\text{M}$ quinidine reduced WT I_{hERG} markedly, with $53.9\pm 2.1\%$ ($n=13$) inhibition of the I_{hERG} tail evident (compatible with prior reports of a submicromolar IC_{50} under similar recording conditions [20,35]). For T618I

I_{hERG} the reduction in current was similar to that seen for the WT current, with $1 \mu\text{M}$ quinidine reducing T618I tail current magnitude by $47.6\pm 5.0\%$ ($n=8$; NS versus WT). A range of quinidine concentrations between 10 nM and $10 \mu\text{M}$ were tested and concentration response relations constructed as shown in Figure 5B. The derived IC_{50} for WT I_{hERG} was $0.64 \mu\text{M}$ (for C.I. and n_H values see Table 1) whilst for T618I I_{hERG} the comparable value was $0.88 \mu\text{M}$. Thus, the IC_{50} for I_{hERG} tail block by quinidine for T618I I_{hERG} was ~ 1.4 -fold that for WT I_{hERG} (see also Table 1).

The Class Ia antiarrhythmic drug disopyramide has been found to be effective against the N588K I_{hERG} SQT1 mutation [20,21], but its effects on T618I hERG are unknown. Therefore we tested the effects of disopyramide on the T618I hERG mutant (Figure 6). Figures 6Ai and Aii show representative I_{hERG} traces in the absence and presence of the drug, with the protocol shown in lower panels. As expected from previous studies [20,26,36], $10 \mu\text{M}$ disopyramide reduced WT I_{hERG} by $55.9\pm 2.6\%$ ($n=13$) whereas it reduced T618I I_{hERG} by $42.9\pm 5.4\%$ ($n=5$, $p<0.05$ versus WT). Three other disopyramide concentrations were tested on T618I mutant channels and concentration response relations constructed as shown in Figure 6B. For T618I I_{hERG} the disopyramide IC_{50} was $16.83 \mu\text{M}$ whilst for WT I_{hERG} inhibition the corresponding value was $7.68 \mu\text{M}$. Thus, the IC_{50} for T618I I_{hERG} tail inhibition by disopyramide was ~ 2.2 fold that for the WT channel.

Similar experiments were also conducted with the Class III antiarrhythmic drug D-sotalol and the Class Ic antiarrhythmic drug flecainide. Figures 6C and 6D show the concentration-response relations for inhibition of WT and T618I I_{hERG} by these drugs. For D-sotalol (Figure 6C) the derived IC_{50} for WT I_{hERG} was $112.2 \mu\text{M}$ whilst for T618I I_{hERG} the comparable value was $356.6 \mu\text{M}$ (~ 3.2 -fold that for WT I_{hERG}). For flecainide, the derived IC_{50} for WT I_{hERG} was $1.87 \mu\text{M}$ whilst that for T618I I_{hERG} was $4.67 \mu\text{M}$ (~ 2.5 -fold that for WT I_{hERG}). Results obtained under conventional voltage clamp for all four drugs are summarized in Table 1.

The limited data currently available on T618I hERG pharmacology appear to suggest some difference in the effect of the mutation on inhibition of pulse and tail currents by $1 \mu\text{M}$ quinidine and $500 \mu\text{M}$ sotalol, during conventional voltage clamp [24]. Ventricular APs involve dynamic changes in membrane potential that influence the profile of observed current; therefore we conducted additional experiments in which concentration-response relations for the 4 drugs examined under conventional voltage clamp were also determined from ventricular AP clamp experiments. For these, the percentage of inhibition of peak I_{hERG} during the AP waveform for three different drug concentrations was calculated for each drug. Concentration-response relations were then constructed as shown in Figure 7. Figures 7Ai and Aii

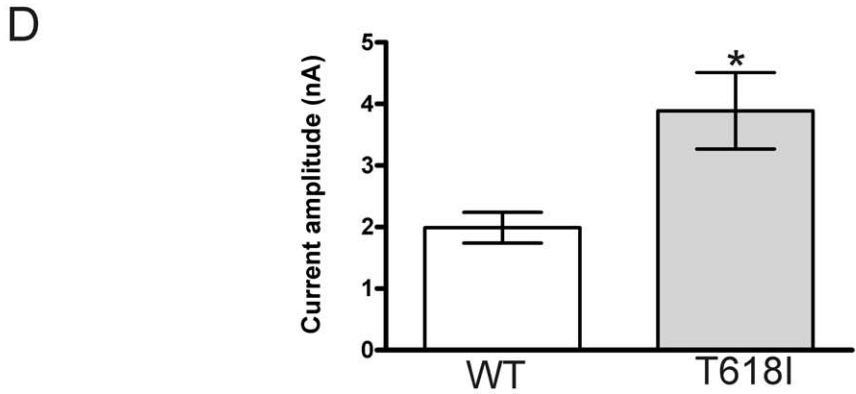
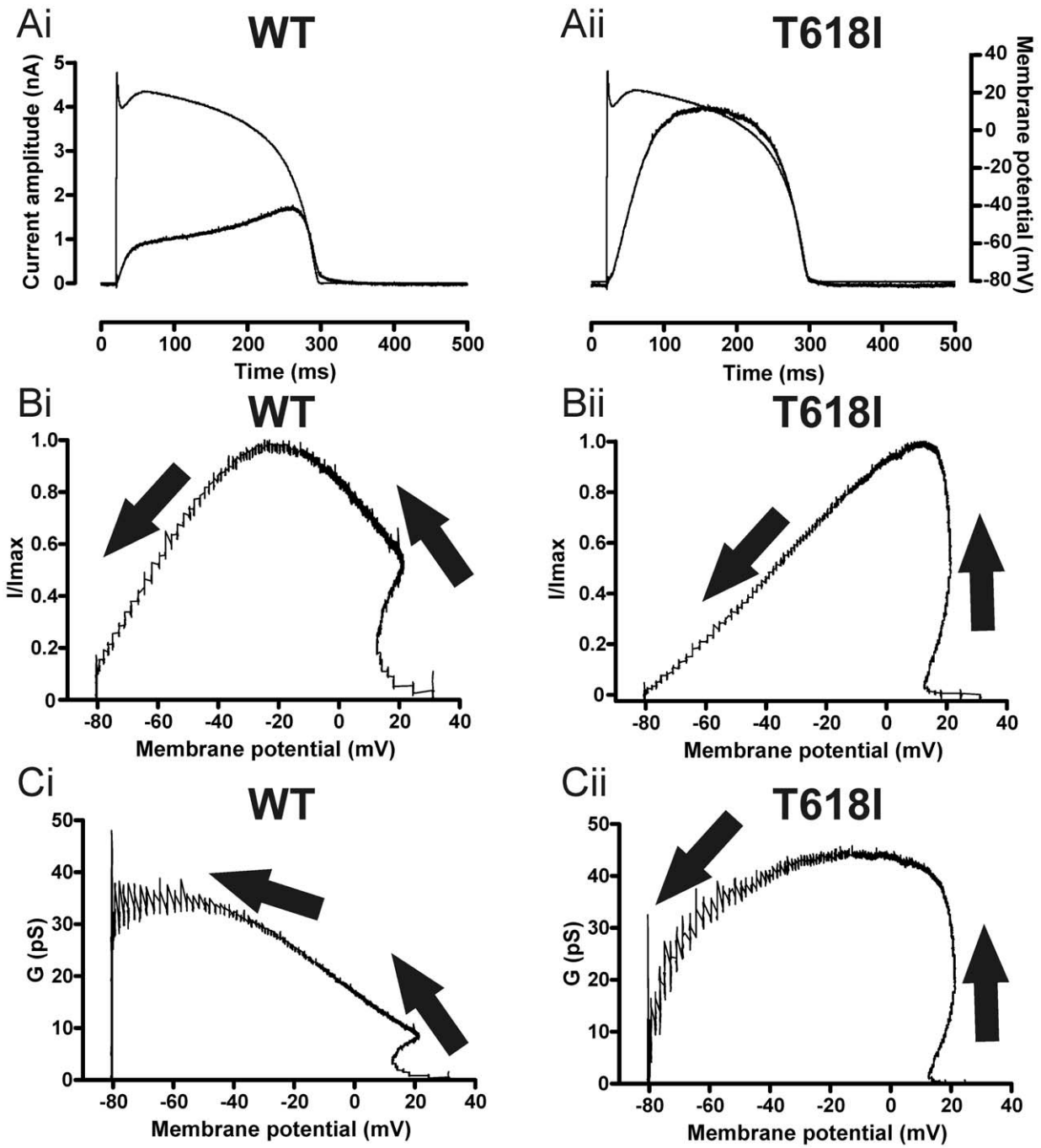


Figure 4. Action potential (AP) voltage clamp of WT and T618I I_{hERG} . (A) I_{hERG} (after p/4 subtraction) elicited by ventricular AP command for WT (Ai) and T618I (Aii) I_{hERG} . Currents are shown overlaid with the voltage protocol. (B) Instantaneous I–V relations for I_{hERG} elicited in A for WT (Bi) and T618I (Bii) I_{hERG} . Current during the repolarising phase of the AP are plotted. Arrows denote direction of repolarisation. (C) Instantaneous conductance-voltage (G–V) relations for I_{hERG} elicited in A for WT (Ci) and T618I (Cii) I_{hERG} during AP repolarisation, Arrows denote direction of repolarisation. (D) Magnitude of peak repolarising current during AP voltage clamp, plotted for WT (n = 14) and T618I (n = 19) I_{hERG} . * denotes statistically significant difference from WT at $p < 0.05$. doi:10.1371/journal.pone.0052451.g004

show representative current traces for WT and T618I I_{hERG} in the presence and absence of quinidine; the ventricular AP command is superimposed over each set of traces. In this example, 1 μM quinidine reduced maximal I_{hERG} during repolarisation by 67% for WT I_{hERG} and 56% for T618I I_{hERG} . Figures 7B–E show concentration-response curves for inhibition of maximal I_{hERG} during repolarisation by quinidine, disopyramide, sotalol and flecainide (Figures 7B–E respectively), whilst Table 2 summarises numerical data for IC_{50} and n_H values. The derived IC_{50} values for WT and T618I I_{hERG} inhibition by quinidine (Figures 7A,B) were, respectively, 0.55 μM and 1.09 μM (~ 2.0 fold the WT value). For disopyramide (Figure 7C), the WT I_{hERG} IC_{50} was 6.47 μM and that for T618I I_{hERG} was 10.65 μM (1.6-fold the WT value). For D-sotalol (Figure 7D) the IC_{50} for WT I_{hERG} was 109.5 μM , whilst that for T618I I_{hERG} was 189.2 μM (~ 1.7 -fold that for WT I_{hERG}). Finally, we found flecainide (Figure 7E) to inhibit WT and T618I I_{hERG} with an IC_{50} of 1.96 μM and of 2.29 μM (1.2 fold the WT value) respectively. Thus, under AP clamp all four drugs exhibited comparatively modest attenuation of their inhibitory action with the T618I mutation.

Discussion

To our knowledge, the present study is the first to have established the effects of the T618I hERG mutation on the profile of I_{hERG} during physiological waveforms. Although limited (single concentration) *in vitro* data have been reported for racemic sotalol and quinidine [24], the present study is the first to provide concentration response data for any drug against T618I hERG and it is also the first to provide any *in vitro* data for T618I I_{hERG} inhibition by disopyramide, D-sotalol and flecainide.

Effects of the T618I Mutation on I_{hERG}

Although the recent study by Sun and colleagues is the first report of the occurrence of the T618I hERG mutation in a clinical context [24], one other investigation has utilised this mutation in the study of the role of a nearby S5 residue (H562) that is able to interact with the pore helix [37]. In that study, T618I I_{hERG} was shown to exhibit both increased currents at positive voltages and reduced tail currents compared to pulse currents following positive voltage commands [37]. These features are in accord with the

subsequent report by Sun and colleagues and with our own data. However, Lees-Miller and colleagues reported a significant ($> +30$ mV) positive shift in I_{hERG} activation $V_{0.5}$ for T618I hERG [37], whilst Sun *et al.* reported a small (~ -5 mV) negative shift in activation $V_{0.5}$ compared to WT I_{hERG} [24]. Both studies were conducted using HEK cells for hERG channel expression, whilst Lees Miller *et al.* performed measurements at 36°C [37] and the recording temperature for the study by Sun *et al.* was not given [24]. Thus, the reason for the apparently opposite observations in the two studies in respect of activation $V_{0.5}$ is not clear. In our experiments, using a similar expression system and recording at 37°C , there was a $+15$ mV shift in activation $V_{0.5}$, which is in good qualitative agreement with the findings of Lees Miller *et al.* [37], but differs from the negative activation shift of $V_{0.5}$ reported by Sun and colleagues [24]. However, unlike Lees-Miller *et al.* [37] and in accord with Sun and colleagues [24], we saw a significant effect of the mutation on I_{hERG} deactivation time-course, with both τ_f and τ_s time constants of T618I I_{hERG} deactivation smaller than those for WT I_{hERG} . Also in accord with Sun and colleagues [24], we did not observe any significant alteration to the rate of I_{hERG} activation for the T618I hERG mutant. The shift in voltage dependence of I_{hERG} inactivation (availability) seen here (Figures 3A,B) is in qualitative agreement with positive shifted inactivation reported by Sun *et al.* [24], as is the positively shifted region of negative slope in the end pulse I–V relation (Figure 1C). However, the extent of positive shift in inactivation $V_{0.5}$ ($\sim +23$ – 25 mV) seen here was smaller than that reported by Sun and colleagues ($\sim +50$ mV); the reason for this difference is at present not clear. Nevertheless, the shift steady-state inactivation seen here is demonstrably sufficient to lead to a significant functional impact: ‘window current’ calculations based on our derived activation and inactivation $V_{0.5}$ and k values revealed significant augmentation, as well as positively shifted peak, of the I_{hERG} window for T618I hERG when compared with WT hERG (Figure 3C). Slowing of time-dependent development of inactivation of I_{hERG} (Figure 3D) may have a synergistic effect in permitting greater I_{hERG} to flow. A modulatory effect of the T618I mutation on I_{hERG} inactivation is not entirely unexpected, given that mutation of the nearby S620 residue (to S620T) has been established to abolish hERG channel inactivation (e.g. [38,39]), although in contrast to the S620T

Table 1. Pharmacology of the T618I hERG mutant studied with conventional voltage clamp.

Drug	WT I_{hERG} IC_{50} (μM)	WT I_{hERG} n_H	T618I I_{hERG} IC_{50} (μM)	T618I I_{hERG} n_H	Fold IC_{50}
Quinidine	0.64 (C.I. 0.51–0.79)	0.65 (C.I. 0.55–0.75)	0.88 (C.I. 0.41–1.88)	0.41 (C.I. 0.25–0.57)	1.4 (0.8–2.4)
Disopyramide	7.68 (C.I. 6.32–9.34)	0.87 (C.I. 0.66–1.07)	16.83 (C.I. 8.56–33.09)	0.47 (C.I. 0.30–0.64)	2.2 (1.4–3.5)
D-Sotalol	112.2 (C.I. 91.7–137.3)	0.74 (C.I. 0.57–0.91)	356.6 (C.I. 305.6–416.1)	0.85 (C.I. 0.70–1.00)	3.2 (3.0–3.3)
Flecainide	1.87 (C.I. 1.56–2.25)	0.81 (C.I. 0.68–0.94)	4.67 (C.I. 3.06–7.13)	0.58 (C.I. 0.45–0.71)	2.5 (2.0–3.2)

IC_{50} and n_H values shown are derived from fits to concentration-response relations in Figures 5 and 6, obtained from fractional inhibition of I_{hERG} using a voltage step protocol (shown in Figures 5A and 6A). Columns show mean values and 95% confidence intervals (C.I.). The right-hand column expresses the ratio of the T618I IC_{50} to the WT IC_{50} value, to one decimal place. The numbers in parentheses in the right hand column represent the range of ratio values for the \pm C.I.s for derived T618I/WT IC_{50} s.

doi:10.1371/journal.pone.0052451.t001

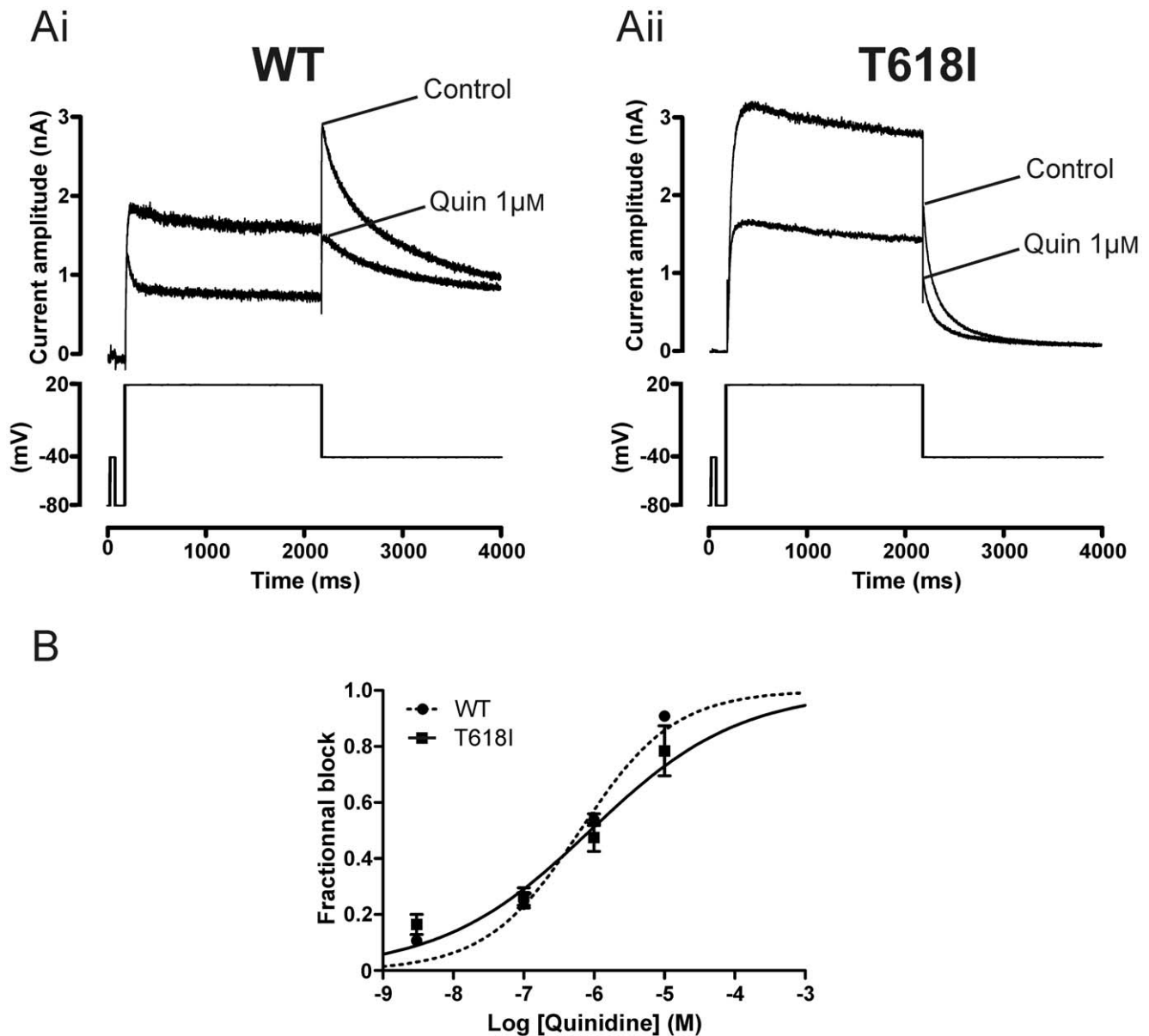


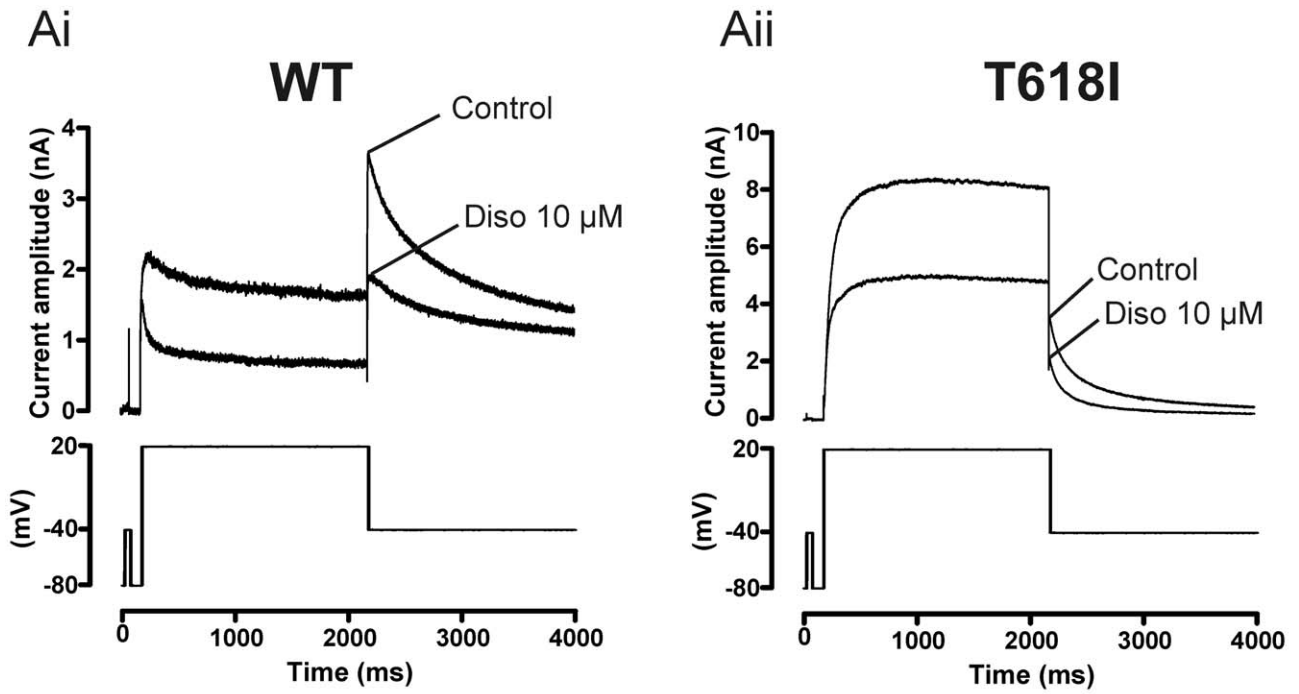
Figure 5. Effect of quinidine on WT and T618I I_{hERG} under conventional voltage clamp. (A) Upper traces show I_{hERG} elicited by voltage protocol shown in the lower panel (applied continuously once every 12 s) in control solution and after exposure to 1 μ M quinidine (Quin). Ai shows data for WT I_{hERG} , whilst Aii shows data for T618I I_{hERG} . (B) Concentration response relations for inhibition of WT and T618I I_{hERG} by quinidine. Fractional inhibition of I_{hERG} was assessed for I_{hERG} tails at each of 4 concentrations (n =at least 5 cells per drug concentration). Steady-state effects were achieved within \sim 2 minutes of drug application and measurements were made at \sim 3 minutes. doi:10.1371/journal.pone.0052451.g005

mutation it is clear that the T618I mutation produces a more modest, partial attenuation of I_{hERG} inactivation.

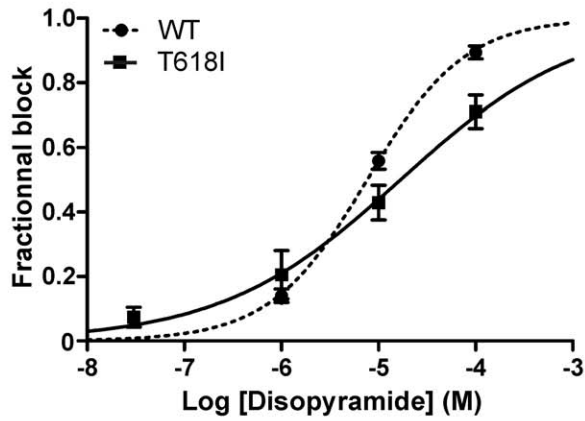
Pharmacology of T618I hERG

It is well established that the inactivation process is important for binding to the hERG channel of a range of drugs, but it is also the case that not all drugs are equally dependent upon inactivation for binding to the channel to occur (e.g. [18,20,21,38–42]). The SQT1 N588K mutation has been shown to lead to markedly elevated IC_{50} values for I_{hERG} blockade by methanesulphonamide compounds including sotalol (20-fold WT I_{hERG} IC_{50} for D-sotalol) and E-4031 (\sim 11.5-fold WT I_{hERG} IC_{50}), whilst those for quinidine (\sim 3.5–6-fold WT I_{hERG} IC_{50}) and disopyramide (1.5–

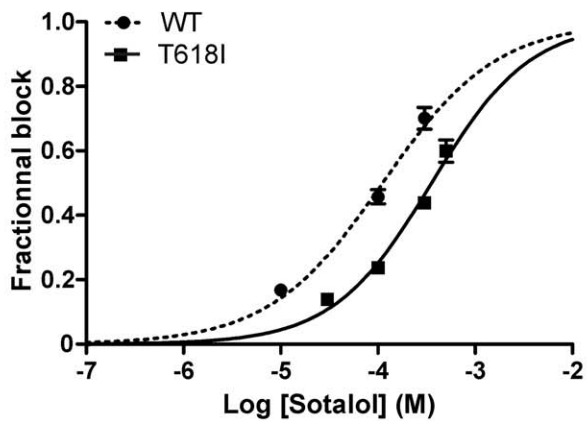
fold WT I_{hERG} IC_{50}) are comparatively little affected [18,20]. In the present study, the T618I hERG mutation elevated the IC_{50} for D-sotalol by \sim 3 fold under conventional voltage clamp, which is substantially less than that seen for N588K hERG [18]. With a voltage protocol similar to that used in the present study, I_{hERG} N588K hERG availability was found to be positively shifted by \sim +62 mV [16]. In the present study, the shift in the voltage dependence of T618I I_{hERG} inactivation was \sim +23–+25 mV. It therefore seems likely that the smaller effect of the T618I mutation in attenuating I_{hERG} block by D-sotalol can be attributed to the ability of the T618I channel to inactivate to a greater extent than has been found to be the case for N588K hERG. In this regard, it is noteworthy that the results of experiments in which different



B



C



D

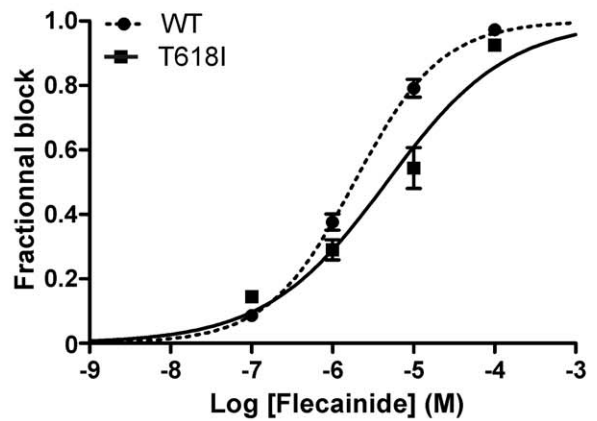


Figure 6. Effect of disopyramide, D-sotalol and flecainide on WT and T618I I_{hERG} under conventional voltage clamp. (A) Upper traces show I_{hERG} elicited by voltage protocol shown in the lower panel in control solution and after exposure to 10 μ M disopyramide (Diso). Ai shows data for WT I_{hERG} , whilst Aii shows data for T618I I_{hERG} . Note different current scales in Ai and Aii. (B) Concentration response relations for inhibition of WT and T618I I_{hERG} by disopyramide. Fractional inhibition of I_{hERG} was assessed for I_{hERG} tails at each of 3 concentrations for WT I_{hERG} ($n = 5$ cells at 1 μ M; 13 at 10 μ M and 5 at 100 μ M; incorporating data from [26], with additional data from a further 8 experiments for 10 μ M disopyramide) and 4 for T618I I_{hERG} ($n = 4$ to 5 cells per concentration). (C) Concentration response relations for inhibition of WT and T618I I_{hERG} by D-sotalol. Fractional inhibition of I_{hERG} was assessed for I_{hERG} tails at each of 3 sotalol concentrations for WT I_{hERG} ($n = 5$ to 9 cells at each concentration) and 4 for T618I I_{hERG} ($n = 5$ to 6 cells per concentration). (D) Concentration response relations for inhibition of WT and T618I I_{hERG} by flecainide. Fractional inhibition of I_{hERG} was assessed for I_{hERG} tails at each of 4 flecainide concentrations for WT I_{hERG} ($n = 5$ to 12 cells per concentration) and T618I I_{hERG} ($n = 5$ to 6 cells per concentration).
doi:10.1371/journal.pone.0052451.g006

inactivation mutations have been combined in order to titrate hERG inactivation suggest that I_{hERG} blocking potency is not related to inactivation in a linear fashion. Thus, for both quinidine and disopyramide single mutations that reduced macroscopic I_{hERG} inactivation to $\sim 20\%$ produced only modest (1.5 and 3.5 fold) reductions in the potency of disopyramide and quinidine, whilst double-mutations that reduced inactivation to $<10\%$ led to elevations of IC_{50} by 6.5 and 7-fold respectively [21]. For T618I hERG in this study, the IC_{50} for quinidine under conventional voltage clamp was ~ 1.4 that of the WT channel, whilst for disopyramide it was ~ 2.2 -fold that of the WT channel. The attenuation of I_{hERG} inactivation by the T618I mutation therefore appears to be insufficient to interfere dramatically with drug binding. At the same time, the greater effect of this mutation on disopyramide's potency under conventional voltage clamp than that seen previously for the N588K mutation (which impairs inactivation to a greater extent than does T618I [15,16,21,24]) suggests that other effects of the mutation on channel conformation as well as upon inactivation *per se* may contribute to its overall effect on disopyramide binding. To our knowledge there are no prior data available on effects of inactivation-attenuating hERG mutants on I_{hERG} blocking potency of flecainide. A prior study from our laboratory has shown that the characteristics of flecainide inhibition of WT I_{hERG} are qualitatively similar to those of the Class Ia antiarrhythmic quinidine and of another Class Ic drug, propafenone [35]. Given that quinidine, disopyramide and propafenone have all been shown to exhibit comparatively little dependence on hERG channel inactivation to exert their inhibitory effects [20,21,36,42] and also that the T618I mutation produced only a modest effect on I_{hERG} blocking potency in this study, it seems reasonable to conclude that hERG channel inactivation is not a major determinant of flecainide potency against hERG. Further experiments on attenuated inactivation mutants are required to determine unequivocally whether or not this is the case.

We also compared between WT and T618I hERG the potency of I_{hERG} inhibition under AP clamp, for each of the drugs studied under conventional voltage clamp. It is known that drug inhibitory

potency against I_{hERG} can vary depending on stimulus protocol [34,43,44]. In our experiments, both stimulus waveform (step versus AP command) and stimulus frequency (repetitive pulsing once every 12 s versus once every second -to apply APs at a physiological rate) differed between the protocols used to obtain the data in Figures 6 and 7. However, the IC_{50} values for WT I_{hERG} inhibition by any of the drugs studied did not differ greatly between conventional and AP clamp protocols (see Tables 1 and 2). In general, however, differences between IC_{50} values obtained with conventional and AP clamp protocols were greater for T618I hERG, although the C.I range for IC_{50} s with the two protocols showed either some overlap (quinidine, disopyramide, D-sotalol) or little separation (flecainide). The range of T618I/WT IC_{50} ratio values was found to be somewhat smaller (1.2–2.0) under AP clamp than under conventional voltage clamp (1.4–3.2), with a marked reduction in this for D-sotalol. Contributory factors to this may be intrinsic voltage-dependence of inhibition [34–36] together with the occurrence (and hence measurement) of peak I_{hERG} at a comparatively positive voltage for T618I compared to WT I_{hERG} during the AP waveform (and compared to the measurement voltage (-40 mV) for T618I I_{hERG} tails under conventional voltage clamp), and a greater sensitivity of drug block to duty-cycle (rate) for the mutant. On the basis of our findings, future detailed investigation of effects of T618I hERG kinetics on channel block are likely to be instructive in this regard, though are beyond the intended scope of the present study.

One puzzling aspect of our pharmacology data is that for the Class I drugs studied, n_H values derived from concentration-response relations obtained under conventional voltage clamp were substantially lower (<0.5 for quinidine and disopyramide) for T618I than for WT I_{hERG} , whilst this was not the case under AP clamp (compare Tables 1 and 2). The low n_H values under conventional voltage clamp do not appear to be attributable to voltage-drop down uncompensated series resistance for T618I I_{hERG} recordings: estimated voltage drop was lower for quinidine (2.31 ± 0.37 mV; $n = 16$) than for D-sotalol (7.61 ± 0.37 mV; $n = 21$), although the n_H value was higher for D-sotalol than for quinidine (Table 1). On the other hand, were the marked

Table 2. Pharmacology of the T618I hERG mutant studied with action potential voltage clamp.

Drug	WT I_{hERG} IC_{50} (μ M)	WT I_{hERG} n_H	T618I I_{hERG} IC_{50} (μ M)	T618I I_{hERG} n_H	Fold IC_{50}
Quinidine	0.55 (C.I. 0.43–0.71)	0.91 (C.I. 0.65–1.18)	1.09 (C.I. 0.82–1.46)	0.92 (C.I. 0.59–1.26)	2.0 (1.9–2.1)
Disopyramide	6.47 (C.I. 3.76–11.12)	0.71 (C.I. 0.40–0.99)	10.65 (C.I. 5.73–19.80)	0.69 (C.I. 0.35–1.05)	1.6 (1.5–1.8)
D-Sotalol	109.5 (C.I. 70.7–169.6)	0.92 (C.I. 0.47–1.37)	189.2 (C.I. 133.3–268.6)	0.90 (C.I. 0.56–1.25)	1.7 (1.6–1.9)
Flecainide	1.96 (C.I. 1.49–2.59)	1.05 (C.I. 0.79–1.30)	2.29 (C.I. 1.72–3.05)	0.86 (C.I. 0.67–1.05)	1.2 (1.1–1.2)

IC_{50} and n_H values shown are derived from fits to concentration-response relations in Figure 7, obtained from fractional inhibition of I_{hERG} using a voltage step protocol (shown in Figure 7A). Columns show mean values and 95% confidence intervals (C.I.). The right-hand column expresses the ratio of the T618I IC_{50} to the WT IC_{50} value, to one decimal place. The numbers in parentheses in the right hand column represent the range of ratio values for the \pm C.I.s for derived T618I/WT IC_{50} s.
doi:10.1371/journal.pone.0052451.t002

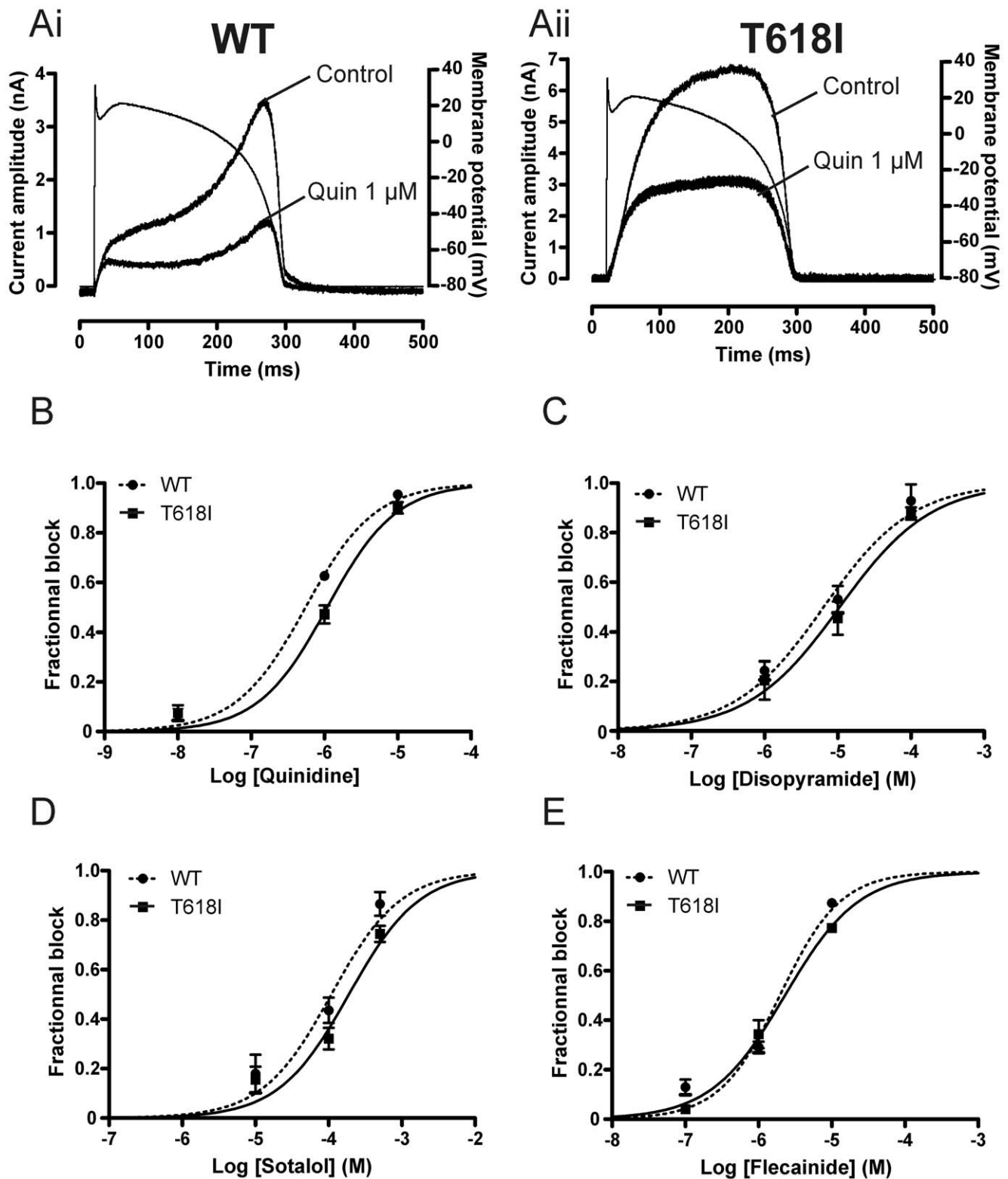


Figure 7. Pharmacology of WT and T618I I_{hERG} under AP voltage clamp. (A) Shows representative traces (after p/4 subtraction) of WT (Ai) and T618I (Aii) I_{hERG} elicited by AP voltage clamp protocol (overlain) in control solution and after exposure to 1 μ M quinidine. Note different current scales in Ai and Aii. AP commands were applied at 1 Hz. (B–D) Concentration response relations for inhibition of WT and T618I peak repolarising current observed during AP clamp by quinidine (B; 3 concentrations tested, n = 4 to 5 cells per concentration); disopyramide (C; 3 concentrations tested, n = 4 to 5 cells per concentration); D-sotalol (D; 3 concentrations tested, n = 4 to 5 cells per concentration); flecainide (E; 3 concentrations tested, n = 4 to 5 cells per concentration).

doi:10.1371/journal.pone.0052451.g007

reduction in n_H for quinidine and disopyramide strongly reflective of altered drug-channel interaction due to the T618I mutation it might be anticipated also to occur for data from AP clamp experiments and this was not the case. The basis for the apparently low n_H for quinidine and disopyramide for T618I I_{hERG} remains unexplained at the present time. Arguably, the more (patho)physiologically relevant pharmacological data are those obtained under AP clamp at a physiologically relevant rate; the major conclusion from those data (Figure 6 and Table 2) is that under these conditions the T618I mutation did not produce a large attenuation of inhibitory potency for any drug studied.

Clinical Relevance

In this study we observed that, under AP clamp, T618I mutant I_{hERG} exhibited an altered current profile, peaking earlier during the AP plateau than was the case for WT I_{hERG} . Previous studies in which the SQT1 N588K hERG mutant has been studied under ventricular AP clamp have shown an inverted U or bow-shaped current profile peaking at $\sim +20$ mV, consistent with the occurrence of little inactivation over physiologically relevant membrane potentials [13,15,16,33]. The N588K hERG mutation produces a greater attenuation of I_{hERG} inactivation than does T618I hERG and our AP clamp data are suggestive of an electrophysiological phenotype for T618I hERG during the ventricular AP that is intermediate between those of WT and N588K I_{hERG} . Accordingly, the effect of the T618I mutation in accelerating ventricular AP repolarisation can also be predicted to be less than that of N588K hERG. This is in agreement with the less extensive QT_c interval shortening for SQT1 patients with the T618I mutation (mean in affected individuals of 316 ms) [24] than those with the N588K mutation (QT_c of ≤ 300 ms in the first two SQT1 genotyped families [13] and a QT of 230 ms in the proband of a third family [14]). The normally slow deactivation of I_{K_r}/I_{hERG} can contribute to resting membrane conductance and protection from premature depolarisation immediately after completion of ventricular AP repolarisation; in pathological settings accelerated I_{K_r} deactivation may increase excitability early in diastole [30,45]. Whether or not the faster deactivation of T618I than WT hERG is able to contribute abbreviated refractory period and susceptibility to programmed stimulation (as clinically observed for SQT1 patients with the T618I mutation [24]) remains to be established, but warrants future *in silico* investigation [30,46].

A first line treatment for the SQTs is the use of implantable defibrillators (ICDs) to protect against sudden death, although ICD use itself carries the risk of inappropriate shocks [47]. A recent report of long term follow up of SQTs patients noted that 58% of patients with ICDs had device-related complications [48]. The same report [48] notes that the T618I SQT1 mutation has now been found in a second family in addition to that originally identified by Sun and colleagues [24]. Pharmacological therapy is therefore attractive both for patients in whom ICDs are not fitted and as an adjunct therapy to reduce arrhythmic events and restore QT intervals towards normal. Our findings extend those previously obtained at a single ($>70\%$ blocking) quinidine concentration [24]; collectively the full concentration response data obtained with both conventional voltage and AP clamp protocols indicate that quinidine largely retains its potency against T618I I_{hERG} . The available *in vitro* data therefore indicate that quinidine

is likely to be beneficial in T618I-linked SQT1. Concordant with this, hydroquinidine has recently been reported to have a positive effect on QT_c intervals in T618I hERG carriers [48]. However, whilst the available evidence from long-term follow up of SQTs patients is that (hydro)quinidine is also effective in arrhythmia prophylaxis [48], diminishing availability of quinidine [49] makes it attractive to find alternative pharmacological therapies for use in SQTs patients. Disopyramide is effective against the N588K mutation *in vitro* [20] and has shown benefits in SQT1 patients [19]. Our experiments indicate that although there is a modest reduction in disopyramide potency for T618I I_{hERG} both during conventional and AP voltage protocols, our data indicate that some I_{hERG}/I_{K_r} blockade can nevertheless be expected to occur within the clinical concentration range ($\sim 6-8 \mu\text{M}$; [50]). Thus, disopyramide may be worthy of investigation as a potential treatment for T618I-linked SQT1. Sun *et al.* have suggested that T618I hERG carriers may be less resistant to drugs like sotalol than had been previously found for N588K-linked SQT1 [24]. Our data with D-sotalol, particularly those obtained under AP voltage clamp, support this proposition; the reduction in I_{hERG} blocking potency of D-sotalol by T618I hERG appears to be substantially less than that produced by N588K hERG [18]. It is possible, therefore, that sotalol may be worthy of clinical investigation for T618I-linked SQT1. Future *in vitro* work may also be warranted to determine whether higher affinity methanesulphonamide Class III drugs than sotalol that are in clinical use (ibutilide, dofetilide) are able to exert some inhibition of T618I at clinically relevant concentrations. Of particular note, flecainide was found to exert marked inhibition of both WT and T618I I_{hERG} at concentrations relevant to clinical serum levels (0.5 to $2.4 \mu\text{M}$; [51]), with little difference between WT and T618I I_{hERG} IC_{50} under AP clamp. Flecainide has been tested previously in a group of SQT1 (N588K hERG) patients unresponsive to sotalol but responsive to hydroquinidine [52]. In that study it was found to produce a small prolongation of QT interval in some patients, which was largely attributable to QRS interval lengthening [52]. To our knowledge, comparable data are lacking in patients with the T618I hERG SQT1 mutation. However, on the basis of our findings flecainide may warrant investigation in this group. Sun and colleagues have also provided evidence that a $>70\%$ blocking concentration of quinidine reduces the inactivation shift for T618I I_{hERG} [24]. However, in our AP clamp experiments none of the drugs studied produced any consistent correction of T618I I_{hERG} profile during a physiological waveform; this suggests that potential benefits of the drugs studied here for QT intervals in patients with the T618I hERG mutation are likely to be attributable to reduction in total repolarising I_{hERG}/I_{K_r} , without restoration of the current's normal time- and voltage- dependent profile during ventricular APs.

Acknowledgments

The authors thank Mrs Lesley Arberry for technical assistance.

Author Contributions

Conceived and designed the experiments: AEH JCH. Performed the experiments: AEH DM YZ. Analyzed the data: AEH DM YZ. Wrote the paper: AEH JCH. Involved in ventricular AP clamp approach used in the study and edited/commented on a completed form of the manuscript: HZ.

References

1. Sanguinetti MC, Jurkiewicz NK (1990) Two components of cardiac delayed rectifier K^+ current. *J Gen Physiol* 96: 195–215.
2. Tamargo J, Caballero R, Gomez R, Valenzuela C, Delpon E (2004) Pharmacology of cardiac potassium channels. *Cardiovasc Res* 62: 9–33.

3. Sanguinetti MC, Jiang C, Curran ME, Keating MT (1995) A mechanistic link between an inherited and an acquired cardiac arrhythmia: HERG encodes the I_{Kr} potassium channel. *Cell* 81: 299–307.
4. Trudeau MC, Warmke JW, Ganetzky B, Robertson GA (1995) HERG, an inward rectifier in the voltage-gated potassium channel family. *Science* 269: 92–95.
5. Weirich J, Antoni H (1998) Rate-dependence of antiarrhythmic and proarrhythmic properties of class I and class III antiarrhythmic drugs. *Basic Res Cardiol* 93 S1: 125–132.
6. Witchel HJ, Hancox JC (2000) Familial and acquired long QT syndrome and the cardiac rapid delayed rectifier potassium channel. *Clinical and Experimental Pharmacology and Physiology* 27: 753–766.
7. Sanguinetti MC, Mitcheson JS (2005) Predicting drug-hERG channel interactions that cause acquired long QT syndrome. *TIPS* 26: 119–124.
8. Hancox JC, McPate MJ, El Harchi A, Zhang YH (2008) The hERG potassium channel and hERG screening for drug-induced torsades de pointes. *Pharmacology and Therapeutics* 119: 118–132.
9. Sanguinetti MC, Tristani-Firouzi M (2006) hERG potassium channels and cardiac arrhythmia. *Nature* 440: 463–469.
10. Modell SM, Lehmann MH (2006) The long QT syndrome family of cardiac ion channelopathies: a HuGE review. *Genet Med* 8: 143–155.
11. Schimpf R, Wolpert C, Gaita F, Giustetto C, Borggrefe M (2005) Short QT syndrome. *Cardiovasc Res* 67: 357–366.
12. Maury P, Extramiana F, Sbragia P, Giustetto C, Schimpf R, et al. (2008) Short QT syndrome. Update on a recent entity. *Arch Cardiovasc Dis* 101: 779–786.
13. Brugada R, Hong K, Dumaine R, Cordeiro J, Gaita F et al. (2004) Sudden death associated with short-QT syndrome linked to mutations in HERG. *Circulation* 109: 30–35.
14. Hong K, Bjerregaard P, Gussak I, Brugada R (2005) Short QT syndrome and atrial fibrillation caused by mutation in KCNH2. *J Cardiovasc Electrophysiol* 16: 394–396.
15. Cordeiro JM, Brugada R, Wu YS, Hong K, Dumaine R (2005) Modulation of I_{Kr} inactivation by mutation N588K in KCNH2: a link to arrhythmogenesis in short QT syndrome. *Cardiovasc Res* 67: 498–509.
16. McPate MJ, Duncan RS, Milnes JT, Witchel HJ, Hancox JC (2005) The N588K-HERG K^+ channel mutation in the ‘short QT syndrome’: mechanism of gain-in-function determined at 37°C. *Biochem Biophys Res Commun* 334: 441–449.
17. Giustetto C, Di MF, Wolpert C, Borggrefe M, Schimpf R, et al. (2006) Short QT syndrome: clinical findings and diagnostic-therapeutic implications. *Eur Heart J* 27: 2440–2447.
18. Wolpert C, Schimpf R, Giustetto C, Antzelevitch C, Cordeiro JM, et al. (2005) Further insights into the effect of quinidine in short QT syndrome caused by a mutation in HERG. *J Cardiovasc Electrophysiol* 16: 54–58.
19. Schimpf R, Veltmann C, Giustetto C, Gaita F, Borggrefe M (2007) In vivo effects of mutant HERG K^+ channel inhibition by disopyramide in patients with a short QT-1 syndrome: a pilot study. *J Cardiovasc Electrophysiol* 18: 1157–1160.
20. McPate MJ, Duncan RS, Witchel HJ, Hancox JC (2006) Disopyramide is an effective inhibitor of mutant HERG K^+ channels involved in variant 1 short QT syndrome. *J Mol Cell Cardiol* 41: 563–566.
21. McPate MJ, Duncan RS, Hancox JC, Witchel HJ (2008) Pharmacology of the short QT syndrome N588K-hERG K^+ channel mutation: differential impact on selected class I and class III antiarrhythmic drugs. *Br J Pharmacol* 155: 957–966.
22. Hassel D, Scholz EP, Trano N, Friedrich O, Just S, et al. (2008) Deficient zebrafish ether-a-go-go-related gene channel gating causes short-QT syndrome in zebrafish *reggae* mutants. *Circulation* 117: 866–875.
23. Zhang YH, Colenso CK, Sessions RB, Dempsey CE, Hancox JC (2011) The hERG K^+ channel S4 domain L532P mutation: characterization at 37°C. *Biochim Biophys Acta* 1808: 2477–2487.
24. Sun Y, Quan XQ, Fromme S, Cox RH, Zhang P, et al. (2011) A novel mutation in the KCNH2 gene associated with short QT syndrome. *J Mol Cell Cardiol* 50: 433–441.
25. Zhou Z, Gong Q, Ye B, Fan Z, Makielski JC, et al. (1998) Properties of HERG channels stably expressed in HEK 293 cells studied at physiological temperature. *Biophys J* 74: 230–241.
26. El Harchi A, Zhang YH, Hussein L, Dempsey CE, Hancox JC (2012). Molecular determinants of hERG potassium channel inhibition by disopyramide. *J Mol Cell Cardiol* 52: 185–195.
27. El Harchi A, McPate MJ, Zhang YH, Zhang H, Hancox JC (2009) Action potential clamp and chloroquine sensitivity of mutant Kir2.1 channels responsible for variant 3 short QT syndrome. *J Mol Cell Cardiol* 137: 83–85.
28. Levi AJ, Hancox JC, Howarth FC, Croker J, Vinnicombe J (1996) A method for making rapid changes of superfusate whilst maintaining temperature at 37°C. *Pflügers Arch* 432: 930–937.
29. Sanguinetti MC, Curran ME, Spector PS (1995). Block of delayed rectifier K^+ channels as an antiarrhythmic mechanism. In: Vereecke J, van Bogaert PP, Verdonck F, editors. Potassium channels in normal and pathological conditions. Leuven University Press. p. 151–66.
30. Du CY, Adeniran I, Cheng H, Zhang YH, El Harchi, et al. (2010) Acidosis Impairs the Protective Role of hERG K^+ Channels Against Premature Stimulation. *J Cardiovasc Electrophysiol* 21: 1160–1169.
31. Smith PL, Baukrowitz T, Yellen G (1996) The inward rectification mechanism of the HERG cardiac potassium channel. *Nature* 379: 833–836.
32. Hancox JC, Levi AJ, Witchel HJ (1998). Time course and voltage dependence of expressed HERG current compared with native ‘rapid’ delayed rectifier K^+ current during the cardiac ventricular action potential. *Pflügers Archiv - European Journal of Physiology* 436: 843–853.
33. McPate MJ, Zhang H, Adeniran I, Cordeiro JM, Witchel HJ, et al. (2009). Comparative effects of the short QT N588K mutation at 37°C on hERG K^+ channel current during ventricular, Purkinje fibre and atrial action potentials: an action potential clamp study. *J Physiol Pharmacol* 60: 23–41.
34. Milnes JT, Witchel HJ, Leaney JL, Leishman DJ, Hancox JC (2010) Investigating dynamic protocol-dependence of hERG potassium channel inhibition at 37°C: Cisapride versus dofetilide. *J Pharmacol Toxicol Methods* 61: 178–191.
35. Paul AA, Witchel HJ, Hancox JC (2002) Inhibition of heterologously expressed HERG potassium channels by flecainide and comparison with quinidine, propafenone and lignocaine. *Br J Pharmacol* 136: 717–729.
36. Paul AA, Witchel HJ, Hancox JC (2001) Inhibition of HERG potassium channel current by the Class 1a antiarrhythmic agent disopyramide. *Biochem Biophys Res Commun* 280: 1243–1250.
37. Lees-Miller JP, Subbotina JO, Guo J, Yarov-Yarovsky V, Noskov SY et al. (2009) Interactions of H562 in the S5 helix with T618 and S621 in the pore helix are important determinants of hERG1 potassium channel structure and function. *Biophys J* 96: 3600–3610.
38. Perrin MJ, Kuchel PW, Campbell TJ, Vandenberg JI (2008) Drug binding to the inactivated state is necessary but not sufficient for high-affinity binding to human ether-à-go-go-related gene channels. *Mol Pharmacol* 74: 1443–1452.
39. Ficker E, Jarolimek W, Kiehn J, Baumann A, Brown AM (1998) Molecular determinants of dofetilide block of HERG K channels. *Circ Res* 82: 386–395.
40. Weerapura M, Hebert TE, Nattel S (2002) Dofetilide block involves interactions with open and inactivated states of HERG channels. *Pflügers Arch* 443: 520–531.
41. Numaguchi H, Mullins FM, Johnson JP Jr, Johns DC, Po SS, et al. (2000) Probing the interaction between inactivation gating and Dd-sotalol block of HERG. *Circ Res* 87: 1012–1018.
42. Lees-Miller JP, Duan Y, Teng GQ, Duff HJ (2000) Molecular determinant of high affinity dofetilide binding to HERG1 expressed in *Xenopus* oocytes: involvement of S6 sites. *Molecular Pharmacology* 57: 367–374.
43. Kirsch GE, Trepakova ES, Brimecombe JC, Sidah SS, Erickson HD, et al. (2004) Variability in the measurement of hERG potassium channel inhibition: effects of temperature and stimulus pattern *J Pharmacol Toxicol Methods* 50: 93–101.
44. Yao JA, Du X, Lu D, Baker RL, Daharsh E, et al. (2005) Estimation of potency of hERG inhibitors: impact of voltage protocol and temperature. *J Pharmacol Toxicol Methods* 52: 146–153.
45. Lu Y, Mahaut-Smith MP, Varghese A, Huang CLH, Kemp PR, et al. (2001) Effects of premature stimulation on HERG channels. *J Physiol* 537.3: 843–851.
46. Adeniran I, McPate MJ, Witchel HJ, Hancox JC, Zhang H (2011) Increased vulnerability of human ventricle to re-entrant excitation in hERG-linked variant 1 short QT syndrome. *PLoS Comput Biol* 7(12): e1002313.
47. Schimpf R, Wolpert C, Bianchi F, Giustetto C, Gaita F, et al. (2003) Congenital short QT syndrome and implantable cardioverter defibrillator treatment: inherent risk for inappropriate shock delivery. *J Cardiovasc Electrophysiol* 14: 1273–1277.
48. Giustetto C, Schimpf R, Mazzanti A, Scrocco C, Maury P, et al. (2011) Long-term follow-up of patients with short QT syndrome. *J Am Coll Cardiol* 58: 587–595.
49. Viskin S, Antzelevitch C, Marquez MF, Belhassen B (2007) Quinidine: a valuable medication joins the list of ‘endangered species’. *Europace* 9(12): 1105–1106.
50. Zema MJ (1984) Serum drug concentration and adverse effects in cardiac patients after administration of a new controlled-release disopyramide preparation. *Ther Drug Monit* 6: 192–198.
51. Breindahl T (2000) Therapeutic drug monitoring of flecainide in serum using high-performance liquid chromatography and electropray mass spectrometry. *J Chromatogr B Biomed Sci Appl* 746: 249–254.
52. Gaita F, Giustetto C, Bianchi F, Schimpf R, Haissaguerre M, et al. (2004) Short QT syndrome: Pharmacological treatment. *J Am Coll Cardiol* 43: 1494–1499.